Chapter 4

Analysis of long-term blazar radio variability

And if the band you're in starts playing different tunes
I'll see you on the dark side of the moon
Pink Floyd, *Brain Damage*

4.1 Introduction

This chapter presents analysis and interpretation of the ATCA monitoring data presented in the previous chapter. Some discussion of techniques for characterising variability is presented in Section 4.2, along with statistics for the long-term variability of all sources. Because the source sample is not subject to a strict set of selection criteria, it is not possible to extend the analysis to a statistically significant interpretation of variability based on optical classification, redshift or other properties. For such comparisons to be made in a meaningful way, it is important to select carefully defined, unbiased source samples. The sources studied here are rather of individual value for investigating blazar variability. Discussion of individual source properties is presented in Section 4.3.

4.2 Analysis of variability

Two important parameters for characterising variability at a particular frequency are the amplitude and time-scale of the variations. In this section, these characteristics for both total and linearly polarized flux density, and their behaviour as a function of frequency, are examined.

4.2.1 Amplitude of variability

Different authors have used various statistics to characterise source variability. For example, Aller (1999) define the "variability index", $S_{\rm var}$, as

$$S_{\rm var} = \frac{S_{\rm max} - S_{\rm min}}{S_{\rm max} + S_{\rm min}},$$

where $S_{\rm max}$ and $S_{\rm min}$ are the maximum and minimum observed flux density, respectively. While $S_{\rm var}$ is a useful measure of the maximum observed fractional variation of a source, the disadvantage of this statistic is that it uses only two points of the entire dataset, the minimum and maximum, and would be largely influenced by outlying measurements.

An alternative statistic is the *modulation index*, μ, defined as the root-mean-square (rms) variation normalised by the average flux density,

$$\mu = \sigma_S / \bar{S} \tag{4.1}$$

The modulation index has been used by various authors to characterise AGN radio variability, (e.g. Quirrenbach et al., 1992; Peng et al., 2000; Kedziora-Chudczer et al., 2001b). The modulation index defined this way makes use of all data, and is influenced by how much time a source spends away from its mean flux density level. In Figure 4.1, μ is plotted against $S_{\rm var}$ for comparison, for all sources in the core sample at all frequencies. The different frequencies are indicated by different symbols, as indicated in the figure. The non-linearity of the dependence of $S_{\rm var}$ on μ is evident in this plot; for large-amplitude modulation, $S_{\rm var}$ asymptotically approaches 1. This is more easily seen in Figure 4.2, which shows μ for polarized flux density plotted against $p_{\rm var}$, the *variability index*, as defined above, for polarized flux density. There is, however, a clear correlation between the two quantities μ and $S_{\rm var}$, despite their quite different definitions. Hereafter, the modulation index defined as the rms fractional variation is used as a measure of source variability, since it uses all data. Modulation indices for both total and linearly polarized flux density are shown in Table 4.1, for all blazars in the core ATCA sample. All of these sources were observed with the ATCA in at least 12 epochs over the three year monitoring program.

Amplitude of variability in linearly polarized flux density

From Figure 4.2 and Table 4.1, it is evident that the fractional variation in polarized flux density is often larger than the fractional variation in total flux density: in one case $\mu_p > 1$, indicating that the rms variations exceed the average linearly polarized flux density. Figure 4.3 shows modulation index for linearly polarized flux density plotted against modulation index for total flux density. This figure shows clearly that in nearly all cases, $\mu_p > \mu_I$.

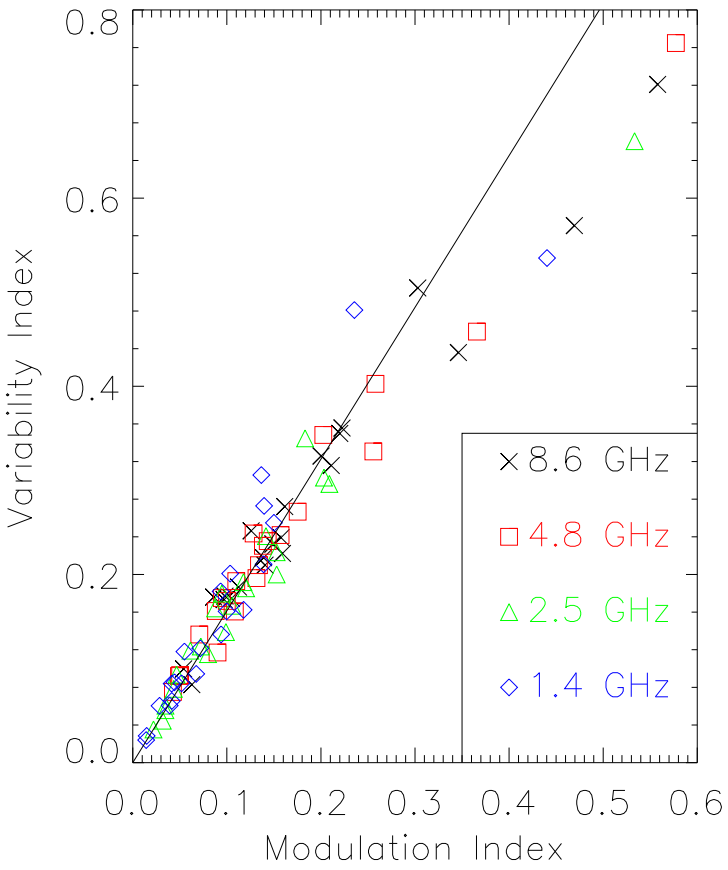

Figure 4.1: Modulation index *vs.* variability index, as defined in Section 4.2.1, for the total flux density of all sources in the core sample for the ATCA blazar monitoring program. Each of the four observed frequencies is indicated by a different symbol.

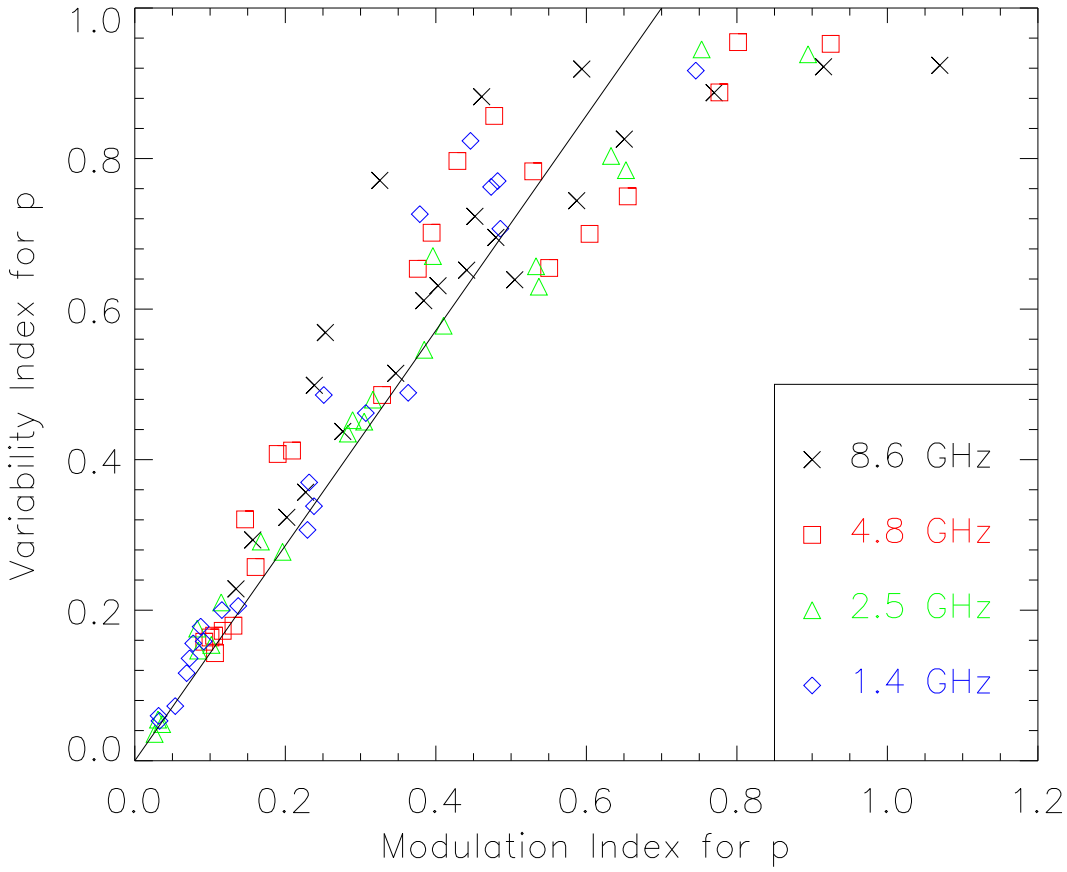

Figure 4.2: Modulation index *vs.* variability index, as defined in Section 4.2.1 for the linearly polarized flux density of all sources in the core sample for the ATCA blazar monitoring program. Each of the four observed frequencies is indicated by a different symbol.

Table 4.1: Modulation indices for total (μ_I) and polarized (μ_p) flux density of the core sample, at each of the four observed frequencies: 1.4, 2.5, 4.8 and 8.6 GHz.

IAU name	μ_I				μ_p			
(B1950)	1.4	2.5	4.8	8.6	1.4	2.5	4.8	8.6
0048−097	0.14	0.15	0.18	0.22	0.49	0.75	0.80	0.65
0208−512	0.05	0.07	0.09	0.20	0.23	0.29	0.11	0.25
0235+164	0.44	0.53	0.58	0.56	0.75	0.89	0.92	1.07
0420−014	0.07	0.05	0.07	0.10	0.23	0.32	0.39	0.33
0430+052	0.09	0.11	0.13	0.16	0.07	0.08	0.16	0.23
0528+134	0.10	0.14	0.16	0.16	0.45	0.65	0.43	0.59
0736+017	0.04	0.06	0.10	0.14	0.05	0.04	0.10	0.20
1144−379	0.24	0.18	0.20	0.22	0.38	0.38	0.53	0.44
1156+295	0.12	0.21	0.37	0.47	0.12	0.28	0.38	0.50
1253−055	0.04	0.09	0.13	0.09	0.07	0.17	0.19	0.92
1519−273	0.14	0.12	0.12	0.12	0.46	0.64	0.55	0.44
1622−253	0.14	0.15	0.26	0.30	0.36	0.53	0.78	0.77
1730−130	0.07	0.10	0.26	0.35	0.24	0.20	0.21	0.40
1741−038	0.14	0.20	0.11	0.13	0.31	0.41	0.65	0.24
1933−400	0.05	0.03	0.05	0.11	0.09	0.08	0.13	0.38
2005−489	0.10	0.09	0.09	0.10	0.47	0.40	0.48	0.59
2149−306	0.03	0.03	0.04	0.06	0.08	0.10	0.11	0.13
2155−304	0.09	0.12	0.14	0.16	0.25	0.30	0.33	0.35
2223−052	0.01	0.04	0.14	0.21	0.03	0.03	0.09	0.16
2230+114	0.01	0.02	0.09	0.14	0.09	0.11	0.12	0.28
2243−123	0.04	0.08	0.13	0.15	0.14	0.54	0.60	0.45
2251+158	0.04	0.03	0.05	0.05	0.03	0.03	0.15	0.48

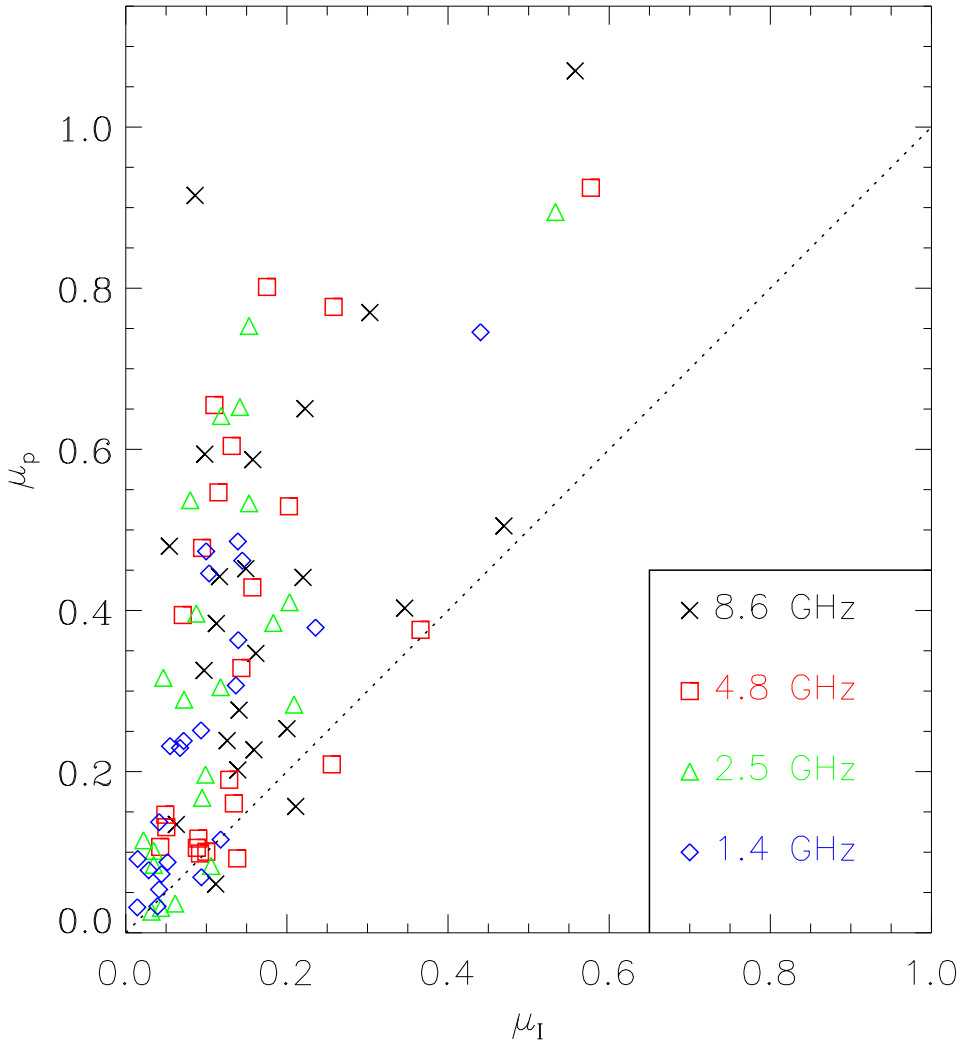

Figure 4.3: Modulation index for total flux density, μ_I, *vs* modulation index for polarized flux density, μ_p, for the core sample at all frequencies. Dotted line shows $\mu_I = \mu_p$.

4.2.2 Time-scales of variability

Neither μ nor $S_{\rm var}$, as defined above, take into account the ordering of the data points. These statistics provide no information on time-scales of variability or rate of change in source flux density. The large range of values for μ is illustrative of the large range of variability behaviour present in this sample of sources, and from inspection of the light curves in Appendix A it is clear that there is a large range of variability time-scales present. The light curves for some sources, e.g. PKS 0048−097 (Figure A.1), PKS 1622−253 (Figure A.12) and PKS 2005−489 (Figure A.16, appear to show multiple "events", i.e. several minima and maxima in the light curves, over the 3-year monitoring period, while for other sources such as NRAO 530 (B1730−130, Figure A.13) and 3C 446 (B2223−052, Figure A.19), only part of an "outburst" is observed during the 3 years. As discussed in Section 3.2.4, strong intraday variability was also observed in three sources. An individual source may exhibit variability on different time-scales; for example, PKS 1622−253 exhibits variability on all time-scales probed by the observations presented here. Clearly, the observable range of time-scales is limited by sampling. The observations are not sensitive to variations on time-scales between one day and two months, or longer than three years. There are a number of methods of characterising time-scales of variability, some of which are investigated below.

Structure function analysis

Structure function analysis is a commonly used method of quantifying time variability. The first order structure function is defined as $D^1(\tau) = \langle [S(t) - S(t+\tau)]^2 \rangle$, where $S(t)$ is the flux density at time t, and τ is lag (Simonetti et al., 1985). Hughes et al. (1992) and Venturi et al. (2001), among others, use the first order structure function to characterise blazar variability. The structure function of a stationary random process is related to the variance, σ^2, and autocorrelation function, $\rho(\tau)$, by $D^1(\tau) = 2\sigma^2[1 - \rho(\tau)]$.

Structure functions have been computed at each frequency for Stokes I, Q, and U, for all sources in the core sample. The method used was as follows (see for example Bondi et al., 1994). Firstly, for each pair of data points i, j, the quantities $t_{ij} = t(i) - t(j)$, and $S_{ij} = [S(i) - S(j)]^2/\sigma_S^2$ were calculated. S_{ij} is normalised by σ_S^2, the variance of the data over the entire observing window, minus the variance expected due to measurement errors. The elements S_{ij} were then binned into time lag intervals, and the average value of S_{ij} for each bin was calculated, to give an estimate of the structure function. A plateau in this normalised structure function corresponding to the time-scale of variations is expected to have an amplitude equal to 2.

The standard error in the determination of the mean S_{ij} for each bin is then calculated as $\sigma = (N-1)^{-1}\{\sum [S_{ij} - \langle S_{ij} \rangle]^2\}^{1/2}$, where N is the number of *independent* samples of the data contributing to each bin. Here only daily average measurements are considered, so there are only 12–15 measurements for each source at each frequency, which means that the number of S_{ij} in each bin is small and the structure functions are rather poorly determined. The error bars shown in Figures 4.4, 4.5 and 4.6 have been calculated simply taking N to be the number of S_{ij} in each bin. This is a good repre-

sentation of the errors if the variations are noise-like, i.e. uncorrelated over successive time samples. However, the data presented here represent a finite sample of a random process with a spectrum which is not that of white noise. In many cases observed here, the total length of the observing period, $T_{\rm obs}$, is not much longer than the characteristic time-scale of the variations, $\tau_{\rm var}$. This contributes an estimation error to the structure function, which increases as $N_{var} = T_{\rm obs}/\tau_{\rm var}$ becomes smaller. A detailed treatment of errors in structure function estimates is presented by Rickett et al. (2000). Only a general discussion of structure function behaviour is presented here, and due to the relatively small number of data points and hence large statistical uncertainties in the structure functions, a more detailed analysis is of somewhat limited use.

Several different behaviours were observed in the structure functions. Firstly, where the time-scale of variability is close to the 3-year time window of the observations, the structure function is observed to rise steadily across the sampled range of time lags, without reaching a plateau. An example of this behaviour is shown in Figure 4.4 for the quasar NRAO 530. For sources whose light curves are dominated by a single outburst, the structure functions are observed to reach a peak at some point, as shown in Figure 4.5 for AO 0235+164. The structure functions for sources which vary on time-scales approximately equal to, or shorter than, the bi-monthly sampling, e.g. PKS 2005−489 (see Figure 4.6), do not have a clearly defined slope at small time lags. For such a small number of data points, structure functions are not particularly meaningful; the effect of limited sampling is more clearly seen from direct inspection of the light curves and it is often easier to interpret the light curves directly.

Rate of change in flux density

The observed rate of change in flux density, dS/dt, is sometimes used to estimate variability time-scale. Definitions of time-scale based on dS/dt have been used, for example, to infer limits on radio source diameters, and to estimate the *variability brightness temperature* from observations. Various definitions of variability time-scale, $t_{\rm var}$, have been used in the literature. McAdam (1978) defines $t_{\rm var} = S_{\rm max}/(dS/dt)_{\rm max}$. Burbidge et al. (1974) and Lähteenmäki & Valtaoja (1999) use $t_{\rm var} = |dt/d(\ln S)|$.

Both of the above definitions weight the fluctuations by their amplitude, but can give an overestimate of the time-scale if, for example, the source contains a large fraction of its flux density in "quiescent", non-variable components. The structure function does not suffer from this problem since it is normalised by the variance of the dataset.

The definitions based on dS/dt, for intrinsic variability, are perhaps most useful for placing limits on the size of an emitting region. If, for example, a significant, monotonic change in flux density has been observed, but the observations do not sample a long enough time range to see minima and maxima in the light curve, then the above definitions for $t_{\rm var}$ extrapolate to give an estimate of the time-scale of variability, assuming the whole source varies. It could also be assumed that some of the source is non-variable; this fraction could perhaps be estimated from VLBI observations. In this case, the estimated "quiescent" flux density is subtracted from the total before calcu-

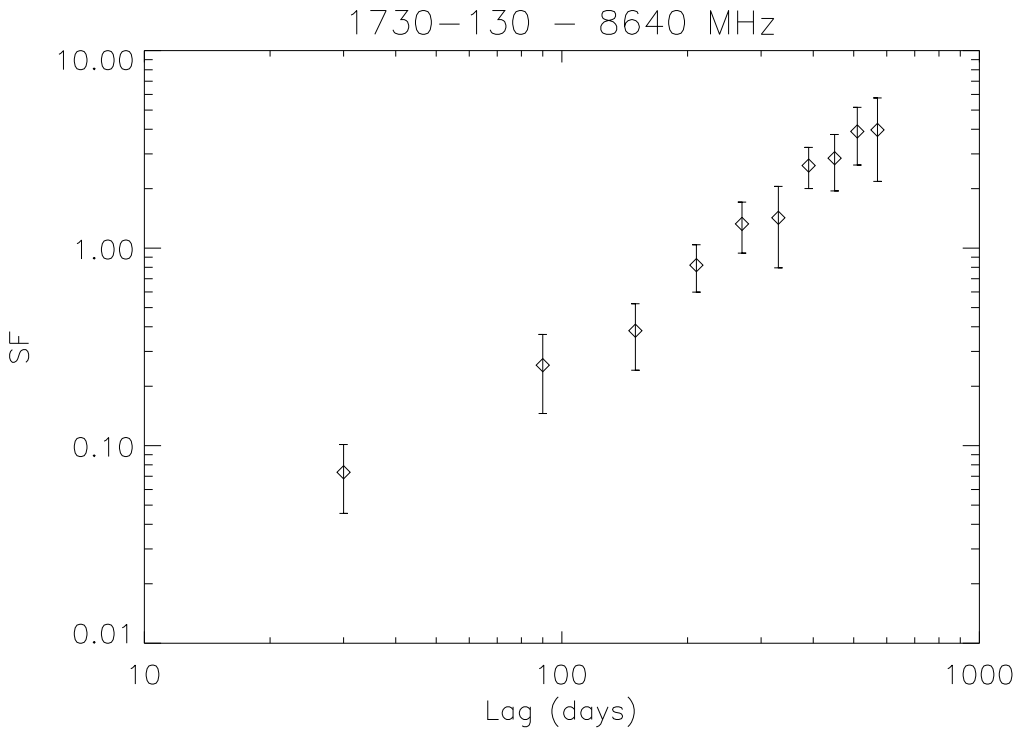

Figure 4.4: Structure function for long-term variability in NRAO 530 at 8.6 GHz

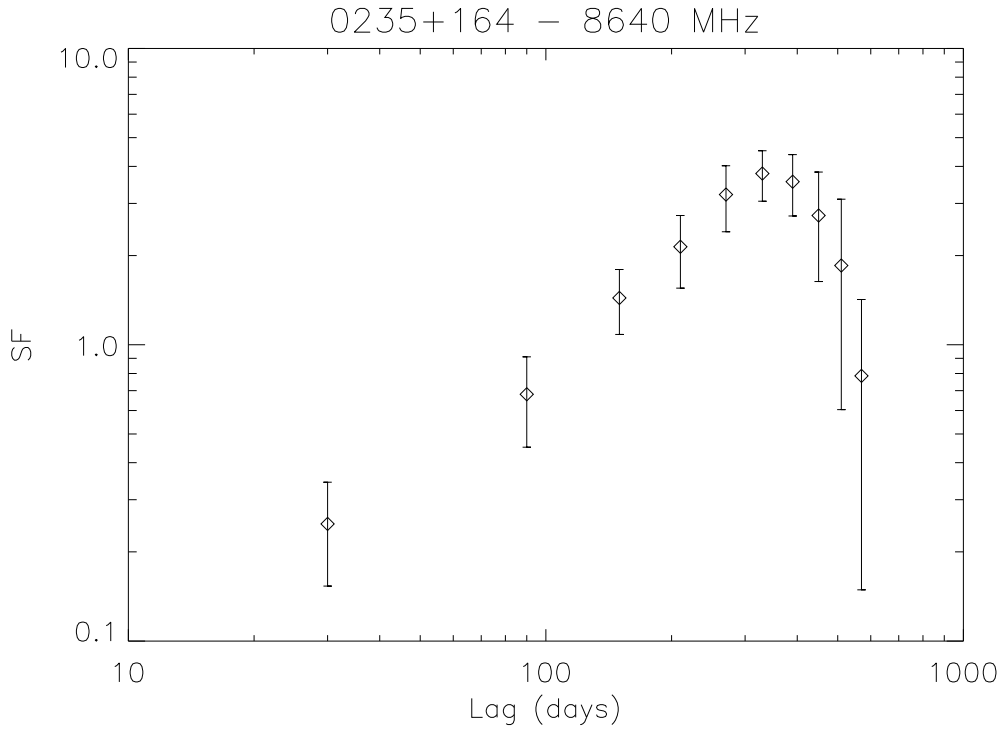

Figure 4.5: Structure function for long-term variability in AO 0235+164 at 8.6 GHz

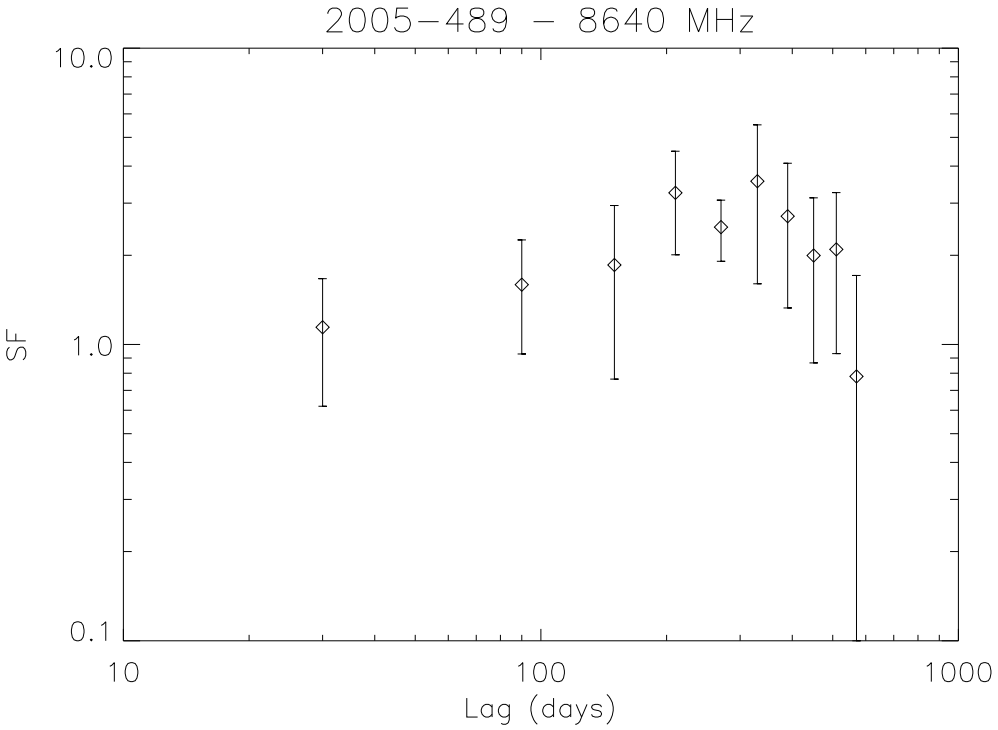

Figure 4.6: Structure function for long-term variability in PKS 2005−489 at 8.6 GHz

lating $t_{\rm var}$. For several sources observed here, time-scales of variability are evidently longer than the three year sampling period.

Counting

Another method for estimating the time-scale of variability is simply counting by eye to estimate the average time between minima and maxima in the light curve. For sparse datasets, this method is just as accurate as more formal estimates. Its main drawback is that identifying minima and maxima in the lightcurves can be somewhat subjective for the case of small-amplitude variations.

The limitations on measurable variability are most easily seen from the light-curves themselves, presented in Appendix A. The variability observed in individual sources is discussed below in Section 4.3, following an investigation of frequency dependence and spectral index effects.

4.2.3 Frequency dependence of variability

Table 4.1 shows that for the majority of sources, the amplitude of variability increases with frequency, for both total and polarized flux density. The dependence of variability on spectral index is also examined. All observed sources have "flat" or inverted spectra, with the mean spectral index $\langle\alpha\rangle > -0.3$ in all cases. Previous studies of large source samples, with a bigger range of spectral index, have found that variability is strongly dependent on spectral index in the sense that flat and inverted spectrum sources are much more variable than steep spectrum (usually defined as $\alpha < -0.5$) sources (e.g. Kesteven et al., 1977).

Is there a correlation between modulation index and spectral index in the blazar sample presented here? Figures 4.7 and 4.8 show mean spectral index versus modulation index at all four frequencies, with both lines of regression from a linear least-squares fit. The regression lines and correlation coefficients have also been calculated for the sample without including the source AO 0235+164, since its modulation indices are significantly larger than those of the other sources, and this source therefore has a large influence on the fitted slopes. The values obtained excluding AO 0235+164 are not shown in the figures, but the effect of leaving out this source does not change any of the conclusions, as discussed below.

For the spectral index calculated between 1.4 and 4.8 GHz, $\alpha_{1.4}^{4.8}$, there is a significant, although not strong, correlation between $\langle\alpha_{1.4}^{4.8}\rangle$ and modulation index at the two lower frequencies, $\mu_{1.4}$ and $\mu_{2.5}$. The correlation coefficient is 0.5, regardless of whether AO 0235+164 is included or not. However, there is no correlation between $\langle\alpha_{1.4}^{4.8}\rangle$ and the modulation index at the two higher frequencies.

For $\alpha_{4.8}^{8.6}$, the spectral index calculated between the two higher frequencies, a similar trend is observed. The correlation coefficients are shown in Figure 4.8. If AO 0235+164 is left out of the regression, these coefficients become 0.41, 0.50, 0.43 and 0.23, at 1.4, 2.5, 4.8 and 8.6 GHz respectively. Thus, there seems to be a significant trend at 1.4, 2.5 and 4.8 GHz, for variability to increase with increasing $\langle\alpha_{4.8}^{8.6}\rangle$. The results suggest

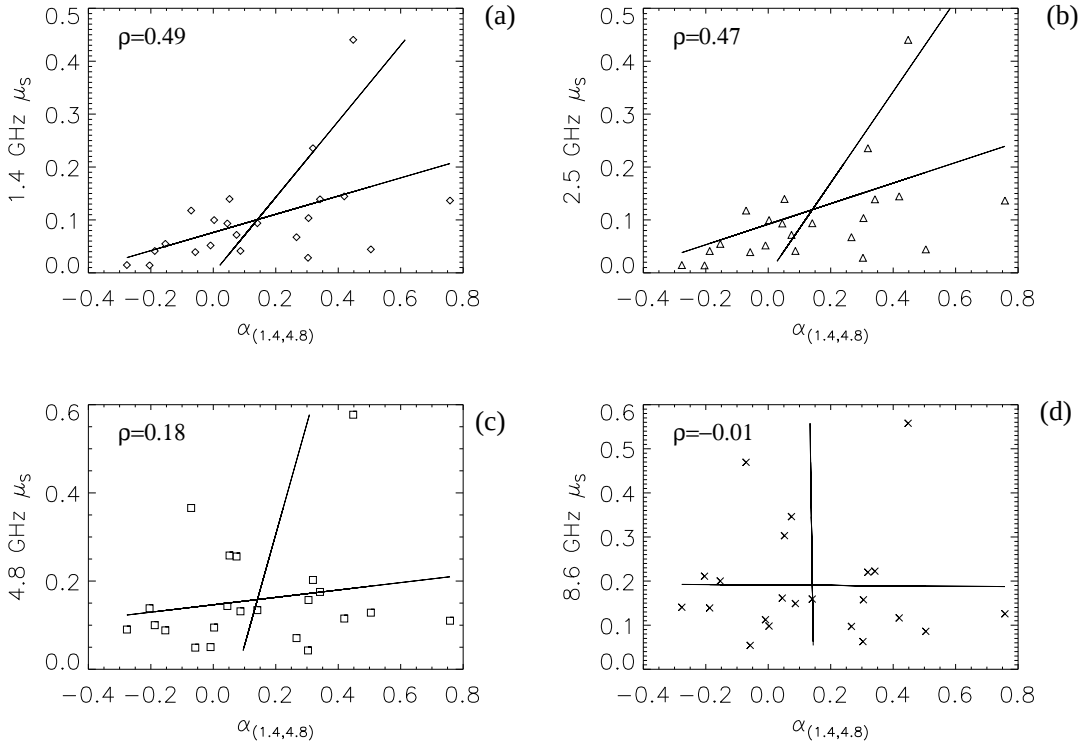

Figure 4.7: Total flux density modulation index at each of the four frequencies, *vs* spectral index between 1.4 and 4.8 GHz. Correlation coefficients, ρ, are shown, and have also been calculated for the sample excluding AO 0235+164. See Section 4.2.3 for discussion.

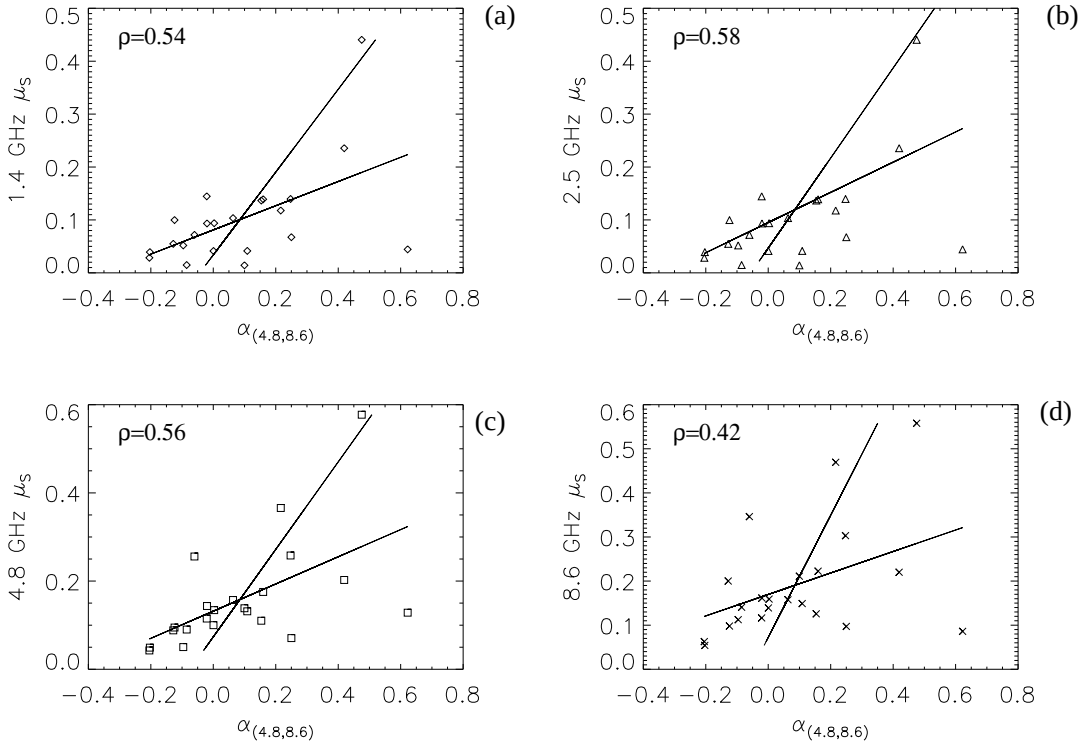

Figure 4.8: Total flux density modulation index at each of the four frequencies, *vs* spectral index between 4.8 and 8.6 GHz. Correlation coefficients, ρ, are shown, and have also been calculated for the sample excluding AO 0235+164. See Section 4.2.3 for discussion.

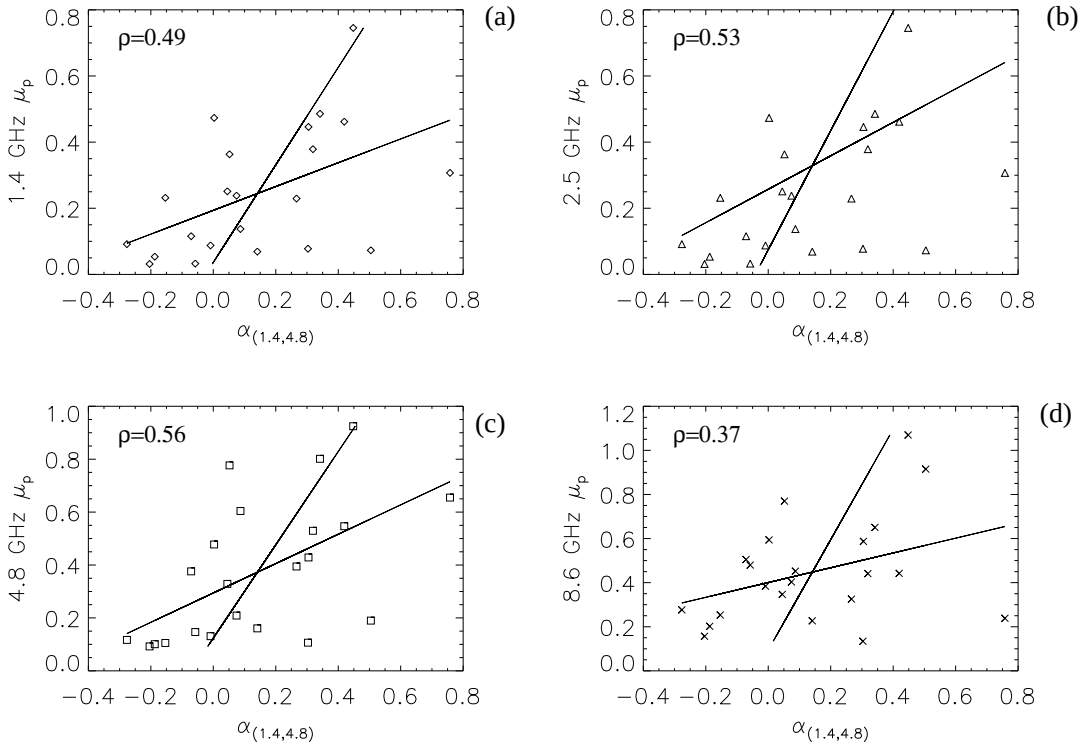

Figure 4.9: Linearly polarized flux density modulation index at each of the four frequencies, *vs* spectral index between 1.4 and 4.8 GHz. Correlation coefficients, ρ, are shown, and have also been calculated for the sample excluding AO 0235+164. See Section 4.2.3 for discussion.

that source variability generally occurs in optically thick components, consistent with previous findings.

Similar results are found for the modulation index in polarized flux density, μ_p, versus the total flux density spectral index, as shown in Figures 4.9 and 4.10. There is no significant correlation between μ_p at 1.4 GHz, and $\langle\alpha_{4.8}^{8.6}\rangle$—ignoring AO 0235+164, the correlation coefficient is reduced to 0.12. There is also no significant correlation between $\langle\alpha_{1.4}^{4.8}\rangle$ and μ_p at 8.6 GHz. There is however, some correlation between $\langle\alpha_{4.8}^{8.6}\rangle$ and μ_p at the two higher frequencies, and between $\langle\alpha_{1.4}^{4.8}\rangle$ and μ_p at the two lower frequencies. These findings show that, similarly to total flux density, variability in polarized flux density in general occurs in components which are optically thick at the observed frequencies.

An important implication of the dependence of variability on spectral index is that, in order to compare variability between different source samples, it is necessary to ensure that the statistics are not biased due to the samples having different spectral index distributions.

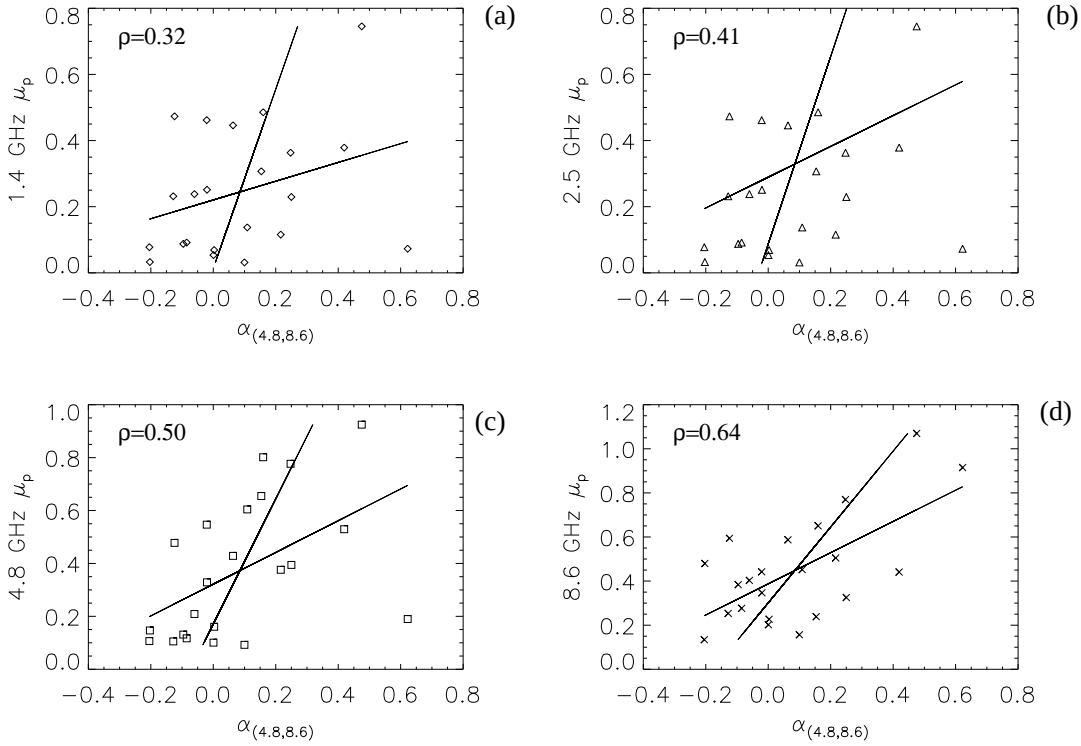

Figure 4.10: Linearly polarized flux density modulation index at each of the four frequencies, *vs* spectral index between 4.8 and 8.6 GHz. Correlation coefficients, ρ, are shown, and have also been calculated for the sample excluding AO 0235+164. See Section 4.2.3 for discussion.

Spectral index variations

The above comparisons used the spectral index averaged over all observations. For some sources, particularly those that show the largest fractional variations, significant changes are observed in the spectral index. These can be seen in the plots of source spectral evolution shown in Appendix A.

A number of sources show "outbursts" which peak first at higher frequencies, and at later times and with lower amplitudes at lower frequencies. Thus, the spectrum becomes more inverted in the early stages of the outburst, and less inverted during the "decay" phase. Such behaviour was noted for a number of flat-spectrum radio sources by Kellermann & Pauliny-Toth (1968). The outburst observed in AO 0235+164 is a classic example of this behaviour, which is consistent with shocks or other disturbances forming in the optically thick base of the jet, and propagating outwards into the optically thin region of the jet (e.g Marscher, 1996).

For some other sources, the spectral index shows only very slight changes despite significant variability, i.e. variability occurs simultaneously across the whole range of frequencies. The clearest example of this behaviour is observed in PKS 2005−489 (Figure A.16), which is further discussed below in Section 4.3.

Some sources, such as PKS 1519−273 (Figure A.11), show rather "messy" long-term light-curves with no clear trends. This is most likely due to variability on time-scales shorter than the bimonthly sampling. PKS 1519−273 is one of the sources which shows large amplitude intra-day variability, and as discussed in Section 1.3.6, this is likely to be predominantly due to interstellar scintillation.

4.2.4 Variability in linear polarization

From a comparison of the total and polarized flux density measurements plotted in Appendix A as a function of time for all sources, it is evident that variations in p, the polarized flux density, are not, in general, straight-forwardly correlated with the variations in S, the total flux density. There is clearly some relationship between the two in many cases, e.g. there is some correlation between the 8.6 GHz variations in p and S for PKS 0048−097 (Figure A.1). Notably, the outburst in AO 0235+164 incurred an increase of more than an order of magnitude in the polarized flux density at 4.8 and 8.6 GHz, which reached a peak at the same time as the total flux density outburst, just before the outburst started to become optically thin (Figure A.3). This is most easily explained as an enhancement/ordering of the magnetic field in a shocked region (e.g Hughes et al., 1989).

Dramatic changes in polarized flux density are often associated with changes in the polarization position angle. An alternative way of visualising changes in polarization, is to plot the path of the **p** vector in the (Q, U) plane, i.e. Stokes U versus Stokes Q. Sometimes this method reveals patterns which can be interpreted using simple models. For example, if the **p** vector is observed to move along a straight line in the (Q, U) plane, this can be fitted by a simple two component model, where one polarized component is non-variable over the observations, and the second component,

which may have a different, but fixed, polarization position angle, varies in intensity. With two or more variable components, the movement of the **p** vector in the (Q, U) plane quickly becomes more complex and introduces many more free parameters. The plots shown in Appendix A reveal that while for some sources, **p** evidently follows a straight line over a few epochs (i.e. a few months or more), the polarization variability is in general complex. This is perhaps not surprising, given the complex structure in linear polarization of blazars revealed in recent VLBI observations (e.g. Homan et al., 2002). Furthermore, the fact that the observed fractional linear polarization is generally only a few percent argues for the presence of turbulent magnetic fields in the radio emitting region (e.g. Jones et al., 1985). Temporal swings in polarization position angle accompanied by large changes in fractional polarization have been modelled as axial compressions associated with shocks (e.g. Hughes et al., 1989; Aller et al., 1996).

In addition to intrinsic changes, interstellar scintillation may have an effect on the measured polarization, even when it does not have a measurable effect on the total flux density. This may complicate modelling of intrinsic variability. Consider for example a source with a very compact, highly polarized component, which would be observed to scintillate, and a more extended, unpolarized component which is too large to scintillate. The scintillating component may contain 100% of the polarized flux density, but only a small fraction of the total intensity. Then the fractional changes in total intensity may be comparable with the fractional measurement errors and hence too small to be measurable, but the fractional changes in polarized intensity may be much larger and easily observable. Scintillation of both total and polarized flux density is studied in more detail in Chapter 5.

4.2.5 Intraday variable sources

How does the long-term variability of a source relate to whether or not it shows intraday variability? Three sources showed highly significant IDV in the present monitoring program, PKS 1144−379, PKS 1519−273, and PKS 1622−253. In addition, large-amplitude intraday variability has been observed for two other sources in the sample during other monitoring programs. Kraus et al. (1999b) reported IDV in AO 0235+164, and this source also showed strong variability over 72 hours in the first epoch of the *Micro-Arcsecond Scintillation-Induced Variability* (MASIV) survey (Lovell et al., 2002, 2003). B1156+295 was another of the strongest variables observed in the MASIV Survey. For both sources, the observed modulation index of IDV in the present ATCA monitoring program, calculated for each session, is typically only 1–2%. Because these two sources are at northern declinations, they are above the horizon for only $\sim 7-8$ hours at the ATCA, and typically only ~ 4 scans were obtained in each epoch of the ATCA monitoring program. The shortest observed time-scales of variability in both AO 0235+164 and B1156+295 are somewhat longer than a day, which means the short-timescale variability in these sources would easily have been missed in the ATCA monitoring program.

The histograms in Figure 4.11 show the modulation index of long-term variability for all sources in the core sample, with shaded areas highlighting the sources in which

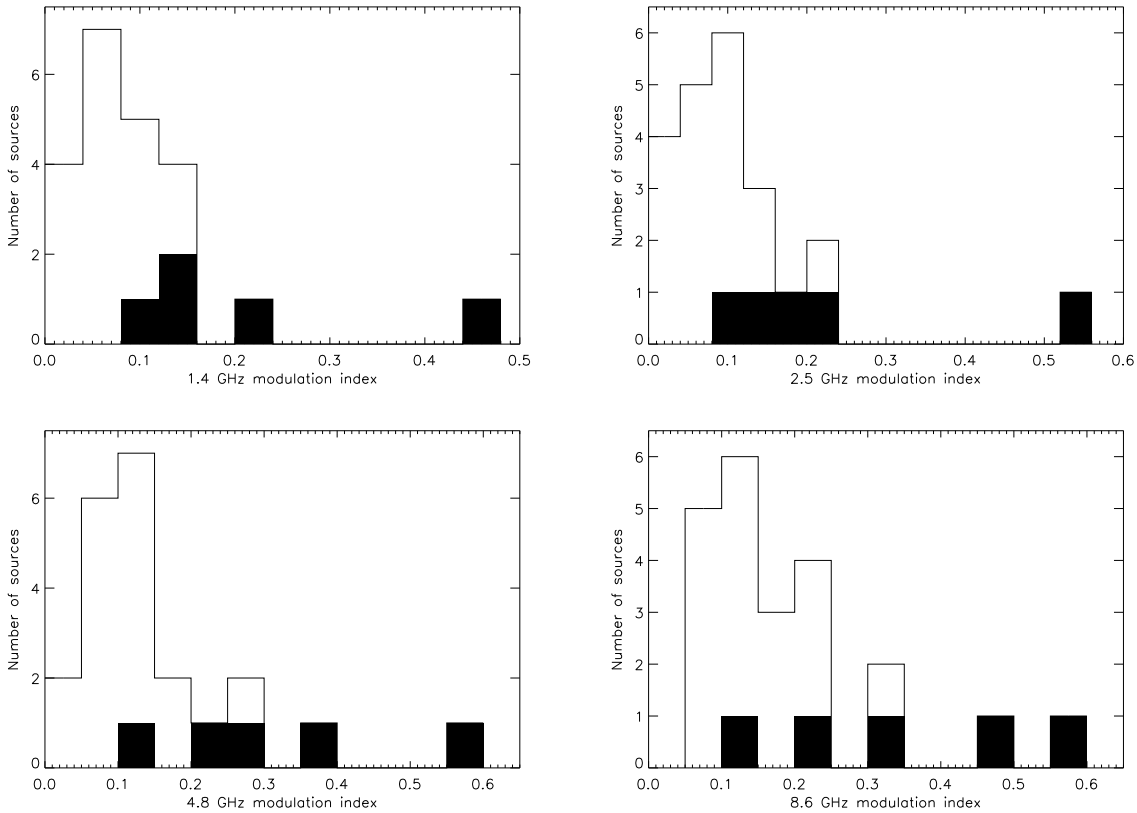

Figure 4.11: Histograms for the modulation index of long-term variability at each of the four frequencies, with shaded areas indicating sources which have shown strong IDV. See Section 4.2.5 for discussion.

strong IDV has been reported. These plots suggest that the sources which show the strongest variability on time-scales of months to years are those most likely to show strong IDV. However, particularly strong and rapid IDV is sometimes observed in sources which do *not* show significant long-term variability, e.g. PKS 1519−273 (see also Chapter 6). This is in agreement with previous findings (Peng et al., 2000; Kedziora-Chudczer et al., 2001b).

The finding that long-term "extreme" variables such as AO 0235+164 and B1156+295 also show variability on time-scales of several days or less is perhaps not surprising, since large-amplitude variability on time-scales of several months indicates highly compact, "core-dominated" sources, which are likely to contain components small enough to be affected by interstellar scintillation. The fact that some long-lived, rapid IDV sources such as PKS 1519−273 do not vary dramatically on longer time-scales suggests that some sources contain very stable, long-lived, extremely compact components, and perhaps that the ISM along certain lines-of-sight is more likely to cause compact sources behind it to scintillate rapidly. For AGN, both source and ISM properties are important in determining whether or not a source will be strongly affected by scintillation.

VLBI observations show that blazars typically contain structure on sub-milliarcsecond

scales. Therefore, interstellar scintillation (ISS) is likely to be important for a number of the observed sources, not just the strong intraday variables. At decimetric wavelengths, sources may show refractive interstellar scintillation on time-scales of weeks to months, even when their angular diameters are large enough to quench ISS at higher frequencies, in the weak scattering regime.

4.3 Notes on Individual Sources

The sources observed in the ATCA blazar monitoring program form an inhomogeneous sample, due to their somewhat random selection. The behaviour of individual sources is of value, rather than the statistics of the sample as a whole. In addition to the data already presented, properties of the individual sources in the core sample are discussed here. Sources identified as EGRET blazars are noted (Fichtel et al., 1994; Thompson et al., 1995; Hartman et al., 1999). The variability patterns observed in each source are briefly discussed, and some historical data are noted. It is worthy of note that many of the flux densities measured recently are not hugely different from those listed in the original Parkes catalogs. This suggests that although significant variability occurs on time-scales of typically several months to several years, sources in general may have a long-term average flux density which is relatively stable, over at least ~ 30 years.

PKS 0048−097

PKS 0048−097 was found in the Parkes Surveys (Wall et al., 1976) with a flux density of 1.4 Jy at 2.7 GHz, and 1.9 Jy at 5 GHz. It is a member of the 1 Jy radio-selected BL Lac sample (Stickel et al., 1991). It has a featureless optical spectrum that has so far eluded firm measurement of a redshift. PKS 0048−097 had a flat or inverted radio spectrum over the three years of ATCA observations, and was strongly variable, with the amplitude of variability being largest at 8.6 GHz. The flux density varies between a minimum and a maximum on a typical time-scale of $\lesssim 200$ days, with the light curve showing several "flares" which appear somewhat blended, and not well sampled by the observations, particularly in the latter half of the monitoring period. The linearly polarized flux density is strongly variable, changing by up to an order of magnitude at 8.6 GHz, with some correlation between the variability in p and I. PKS 0048−097 was included in the 4-year monitoring program of Venturi et al. (2001), who report that it was also observed with the VLBA at 8.4 and 22 GHz, achieving angular resolution $\lesssim 1$ mas, and found to be unresolved at both frequencies. PKS 0048−097 was not detected by EGRET.

PKS 0208−512

PKS 0208−512 was optically identified as a 17th magnitude quasar at z=1.003 (Peterson et al., 1976), and found to have high optical polarization, measured to be $> 10\%$, by Impey & Tapia (1988). More recently, a redshift of 0.999 was measured by Wisotzki et al. (2000). The source is associated with a strong ($> 5\sigma$) EGRET detection (Bertsch

et al., 1993; von Montigny et al., 1995), and showed evidence of strong variability in γ-rays > 100 MeV. In 1998 December, the source was re-observed with EGRET, but was evidently much weaker, with upper limits well below the previous strong detections (G. Kanbach 1998, private communication).

Flux densities for PKS 0208−512 measured in the original Parkes Surveys (Wall et al., 1975) were 3.6 Jy at 2.7 GHz, and 3.2 Jy at 5 GHz; not significantly different from the ATCA flux densities observed for most of the ATCA monitoring presented here, although the flux density has been observed to vary substantially on time-scales of several years (e.g. Tzioumis, 1987). In the 2000 June session of the ATCA monitoring program, the 8.6 GHz flux density had increased by a factor of two, more than 2 Jy, since the previous observing session in 1999 August. The 4.8 GHz flux density had also increased by ~ 1 Jy, so that the source had gone from having a slightly steep (optically thin) spectrum, to an inverted spectrum. More recent observations of the source at 4.8 and 8.6 GHz, from mid-2001 to early 2002, show the flux density to have declined again, from 4.4 Jy to 3.5 Jy at 8.6 GHz. Therefore, the outburst probably peaked between mid-2000 and mid-2001. Clearly, most of the cm wavelength activity in PKS 0208−512 occurs on time-scales of several years, longer than the period of monitoring presented here.

At the other end of the spectrum, the source flux in the EGRET energy band has been reported to change by a factor of 2–3 on time-scales of order 10 days (von Montigny et al., 1995). This behaviour is very different from the radio and illustrates the difficulty of connecting blazar variability across the entire electromagnetic spectrum, short of sampling all intermediate wavelengths over a long period of time. While quasi-continuous monitoring might be feasible for small, dedicated, ground-based telescopes, it is not realistically possible for expensive, multi-target satellite experiments. While one could speculate that the recent radio outburst might be physically connected with the earlier, strong γ-ray activity, with a time-delay of several years for the "burst" to propagate out to the parsec-scale radio jet, there is no conclusive evidence one way or the other to support such a hypothesis.

AO 0235+164

AO 0235+164 has been intensively studied at many wavelengths over the past 30 years. Spinrad & Smith (1975) first reported the source to be a radio and optical variable, and identified it as a BL Lacertae type object due to its variability and featureless optical spectrum. However, Nilsson et al. (1996) reported that during an optical minimum, the optical spectrum was that of a highly polarized quasar. AO 0235+164 was detected by EGRET (Thompson et al., 1995). Correlated radio and optical variability on time-scales of months has been reported (e.g. Ledden et al., 1976), although not all optical flares can be associated with a radio flare (e.g. Roy et al., 2000). Some evidence for periodic radio variations on a time-scale of several years has been claimed (e.g. Roy et al., 2000).

Very rapid, unusual radio variability was reported by Kraus et al. (1999b), and the authors investigate several possible mechanisms to explain the observed variations.

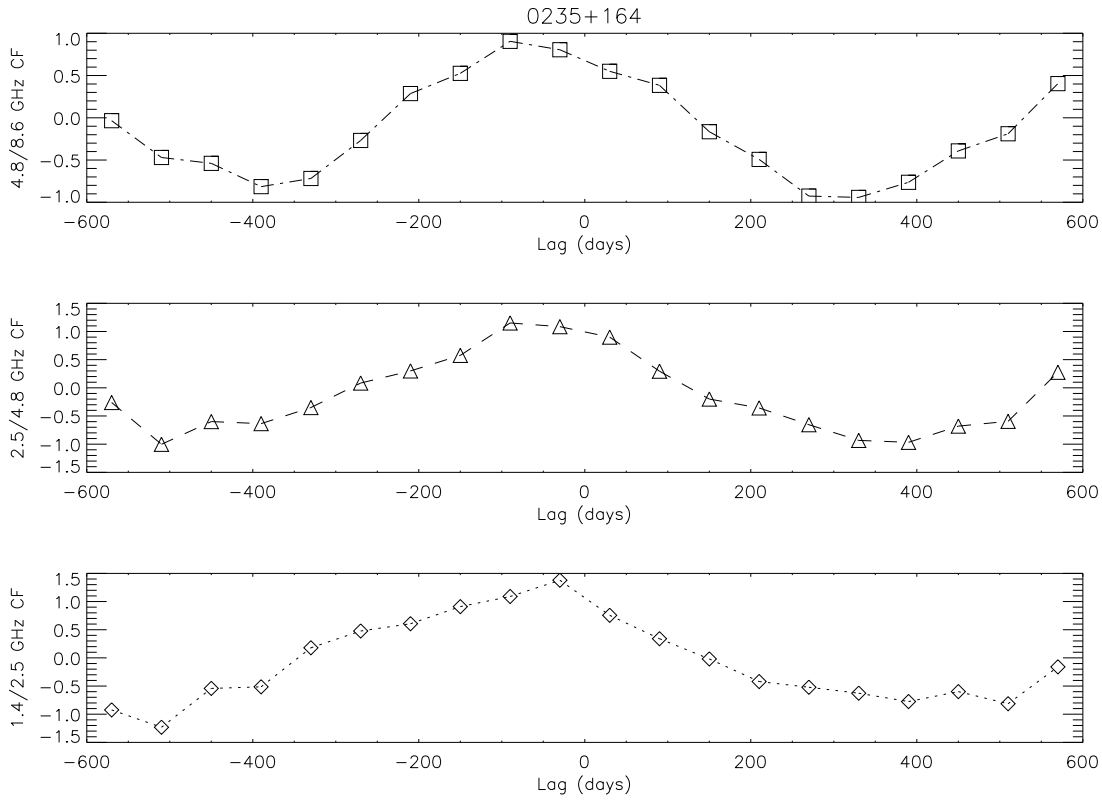

Figure 4.12: Discrete cross-correlation functions for the total flux density, for AO 0235+164. Top panel shows the cross-correlation between the 4.8 and 8.6 GHz variations; middle panel shows 2.5 and 4.8 GHz; and bottom panel shows the cross-correlation between 1.4 and 2.5 GHz. A peak at negative lag indicates that the higher frequency leads the lower.

Rapid variability at 5 GHz was also observed during the recent MASIV VLA Survey (Lovell et al., 2002, 2003). Being such a compact radio source (e.g. Frey et al., 2000), AO 0235+164 is likely to be affected by interstellar scintillation.

AO 0235+164 showed by far the largest amplitude variability of any observed in the ATCA monitoring program. A huge outburst occurred during 1997–1998. The outburst was observed to peak at 8.6 GHz first, and at later times and with decreasing amplitude towards the lower frequencies. The delay between frequencies is evident in the light curves presented in Appendix A, and also in the cross-correlation functions, shown in Figure 4.12. Webb et al. (2000) suggested that the optical-to-radio outburst observed in AO 0235+164 in 1997 may be a result of gravitational microlensing, but this scenario does not explain the observed delay between high and low radio frequencies. The four-frequency radio data presented here show opacity effects, more consistent with models of intrinsic variability due to a shock wave which propagates outwards from the base of the jet (e.g. Marscher, 1996). At each frequency, the linearly polarized flux density, p, reached a peak around the same time as the total flux density. p increased by more than an order of magnitude at the two higher frequencies, with a narrower

peak than the total flux density. AO 0235+164 was also monitored between 1996 and 1999 with the Medicina and Noto telescopes (Venturi et al., 2001), and with the VLBA at 8.4 and 22 GHz. Venturi et al. (2001) report that the source was unresolved at both frequencies, on a scale of $\lesssim 1$ mas.

PKS 0420−014

Bolton & Ekers (1966) identified PKS 0420−014 (Wall et al., 1971) as an 18th magnitude quasar at $z = 0.915$. It shows high optical polarization (Brindle et al., 1986). PKS 0420−014 was also detected by EGRET (Radecke et al., 1995). The ATCA monitoring showed a strong, inverted spectrum radio source displaying 10% rms fractional variability at 8.6 GHz, over the three years of monitoring. The polarized flux density variations are fractionally larger, rms $\sim 30\%$ or more. Large-amplitude variability has been observed with the University of Michigan 26 m antenna (e.g. Aller et al., 1985), on time-scales of typically several years.

3C 120 (PKS B0430+052)

Variability in the radio galaxy 3C 120 has been well-studied since the 1960s. During the ATCA monitoring program, the source showed one of the "classical" outbursts similar to that shown in the early review paper by Kellermann & Pauliny-Toth (1968), which could be explained by the model of van der Laan (1966), for a uniformly expanding spherical source. In this source, unlike most of the others observed, the fractional polarized flux density changes are not much larger than the fractional total flux density changes, indicating that a large fraction of the polarized flux density is in "quiescent" components. 3C 120 is not an EGRET source.

PKS 0528+134

PKS 0528+134 is another EGRET-detected blazar, which has been extensively studied at various wavelengths. The flux densities listed in the original Parkes catalog (Shimmins et al., 1975) are 3.0 Jy at 2.7 GHz, and 3.9 Jy at 5 GHz. During the ATCA monitoring program, the flux densities at 8.6 and 4.8 GHz showed a fairly smooth decrease over the first few months, then a slight increase in mid-1998, the peak of which was somewhat undersampled by the observations. The linearly polarized flux density at 4.8 and 8.6 GHz showed a sharp decrease in mid-1998. The variability at the two lower frequencies does not show any significant correlation with the higher frequency variability, and the 1.4 GHz variability in particular has a stochastic pattern which could be a result of refractive interstellar scintillation (e.g. Rickett et al., 1984). Pohl et al. (1995) report that PKS 0528+134 was subject to an extreme scattering event in mid-1993, and note the likely importance of interstellar scattering for this source. Data presented by Peng et al. (2001) from long-term monitoring of PKS 0528+134 with the Effelsberg 100 m telescope, show that the source underwent a large radio outburst prior to the start of the ATCA monitoring program, during 1995–1996.

PKS 0736+017

PKS 0736+017 is identified as a relatively low-redshift, $z = 0.191$, 18th magnitude quasar (Wall et al., 1971, and references therein). This source had a slightly optically thin spectrum during the ATCA monitoring program, probably indicating significant, steep spectrum, extended emission around the compact core. Variability in both total and polarized flux density was observed, although the polarization position angle remained stable, within $\sim 10°$, at all observed frequencies. Not detected by EGRET.

PKS 1144−379

PKS 1144−379 was noted to be a radio variable in the catalogue for the Parkes 2700 MHz survey (Fifth part, Bolton & Shimmins, 1973). It is a member of the 1 Jy sample of BL Lac objects (Stickel et al., 1991). As discussed earlier, it is a strong intraday variable in both total and polarized flux density (Kedziora-Chudczer et al., 2001b, and this thesis). In addition to the IDV, PKS 1144−379 showed variations on longer time-scales during the ATCA monitoring program, which were somewhat undersampled by the observations. The polarized flux density showed large and rapid variations on time-scales shorter than the sampling interval. VLBI observations including the Hartebeesthoek antenna indicate that PKS 1144−379 has a very strong, compact core. The IDV is most easily explained as interstellar scintillation, while the observed variations on time-scales of several months may well be intrinsic. It is not clear what are the longest time-scales of scintillation and the shortest time-scales of intrinsic variability for PKS 1144−379, particularly for the polarized flux density which shows large changes from session to session. Not detected by EGRET.

B2 1156+295

Listed in the Second Bologna source catalogue (Colla et al., 1970), B2 1156+295 was the second-most variable source observed in the ATCA monitoring program. The light-curve clearly shows two peaks at 8.6 GHz, which do not appear to be "resolved" at 2.5 and 1.4 GHz, although the light-curve is undersampled in the latter half of the monitoring period. At the lower frequencies, the time-scales of variability are much longer, and there are delays between the increase in flux density from high to low frequencies, indicating opacity effects in the source. A large increase in polarized flux density at 8.6 GHz is observed, coincident with the second peak in total intensity. The spectrum changed from slightly steep to inverted during the outburst, and was steepening again by the observation of 2000 June. This source also showed IDV in the first epoch of the MASIV Survey (Lovell et al., 2002, 2003), although it did not show significant IDV (modulation index typically 1–2%) during the ATCA monitoring program. The high northern declination of the source means that only a few scans over several hours were obtained during each ATCA observing session. B2 1156+295 is an EGRET blazar.

3C 279 (B1253−055)

Of all sources in the sample presented here, 3C 279 is perhaps the most well-studied across the electromagnetic spectrum. It was detected by EGRET (Bertsch et al., 1991), and has been subject to numerous multiwavelength studies (e.g. Grandi et al., 1995; Hartman et al., 2001). Wardle et al. (1998) used the observation of circularly polarized radio emission from 3C 279 to argue for the presence of an electron-positron jet. The ATCA light curves show a very strong, inverted spectrum source. Perhaps the most notable feature observed during the present program was the increase in linearly polarized flux density at 8.6 GHz between late 1998 and mid-2000, from less than 0.5 Jy to more than 2 Jy. 2 Jy is $\sim 10\%$ of the total flux density.

PKS 1519−273

Peterson et al. (1973) identified PKS 1519−273 with an 18th magnitude quasi-stellar object. It a BL Lac object with a featureless spectrum, that has so far eluded measurement of a redshift. Flux densities listed in the Parkes catalog (Bolton et al., 1975) are 2.0 Jy at 2.7 GHz, and 2.3 Jy at 5 GHz. It is one of the most extreme, long-lived intraday variable sources known (Kedziora-Chudczer et al., 2001b), and shows an unusually high fraction of circular polarization (Macquart et al., 2000). Because the IDV was somewhat poorly sampled for the one-day observations presented here, the long-term average flux density measurements are subject to large uncertainties, depending on whether the source was observed near a minimum or a maximum in its IDV pattern. A more detailed study of IDV in PKS 1519−273, and of longer-term trends, is presented in Chapter 5. PKS 1519−273 is not an EGRET source.

PKS 1622−253

PKS 1622−253 was detected by EGRET (e.g. Nolan et al., 1996). It has been classified as a low-polarization quasar in the optical (Impey & Tapia, 1990), but Stickel et al. (1994) suggest that this measurement probably refers to a nearby, brighter object. PKS 1622−253 is optically very faint, 20th magnitude (Stickel et al., 1994), and lies in a heavily obscured field. A redshift of $z = 0.786$ was measured by di Serego-Alighieri et al. (1994). The original Parkes catalog flux densities are 2.3 Jy at 2.7 GHz, and 2.0 Jy at 5 GHz (Bolton et al., 1975). The source has curious arcsecond radio structure, with steep-spectrum extended components on both the eastern and western sides of the core (see Figure 3.2). A VLBA image at 8.4 GHz, published by Tingay et al. (1998), shows only a compact core with a weak jet-like feature extending ~ 2 mas to the northwest. The original Parkes catalog flux densities are 2.3 Jy at 2.7 GHz, and 2.0 Jy at 5 GHz (Bolton et al., 1975). PKS 1622−253 is a strong IDV source, at least some of the time, and also shows large amplitude variability in both total and polarized flux density, particularly at 8.6 GHz, on a time-scale of months, which is probably intrinsic to the source. The variability is not well-sampled by the ATCA observations presented here. The IDV in PKS 1622−253 is further studied in Chapter 5.

NRAO 530 (B1730−130)

NRAO 530 (Pauliny-Toth et al., 1966) is a strong radio source which has been well studied for many years. It has one of the highest brightness temperatures measured with VSOP, $\sim 3 \times 10^{12}$ K (Bower & Backer, 1998), and is listed as a γ-ray blazar in the Third EGRET catalog (Hartman et al., 1999). The ATCA monitoring showed NRAO 530 to be highly variable on time-scales of years, longer than probed by the observations presented here. An unusual, mm-wavelength flare in mid-1995 was reported by Bower et al. (1995). The decrease in flux density seen from the beginning of the ATCA monitoring program is likely to be the tail-end of this outburst. A peak in polarized flux density is seen in mid-1997 at 8.6 and 4.8 GHz, after the source spectrum started to become optically thin. At 4.8 and 8.6 GHz, the polarization position angle varied by $\sim 30^\circ$ during the ATCA monitoring, while remaining constant to within a few degrees at 1.4 and 2.5 GHz.

PKS 1741−038

PKS 1741−038 is a quasar at $z = 1.054$ (White et al., 1988) which was detected by EGRET (Hartman et al., 1999). Quirrenbach et al. (1992) report variability on a time-scale of several days. Hjellming & Narayan (1986) interpreted unusually strong variability at 1.49 GHz as refractive interstellar scintillation. PKS 1741−038 underwent an extreme scattering event in 1992 (Fiedler et al., 1992). The ATCA measurements show an inverted-spectrum source with time-scales of variability evidently longer than the three year monitoring program, although smaller fluctuations on shorter time-scales are evident. The polarized flux densities at 4.8 and 8.6 GHz changed by factors of 3 or more during the ATCA monitoring program.

PKS 1933−400

PKS 1933−400 was identified as a 19th magnitude quasar (Wall & Cannon, 1973) with the original Parkes catalog flux densities listed as 1.2 Jy at 2.7 GHz, and 1.4 Jy at 5 GHz. The ATCA observations showed an initially very flat-spectrum source which became more optically thin over the three years of monitoring. This source also appears as a γ-ray emitter in the EGRET catalog (Thompson et al., 1995).

PKS 2005−489

PKS 2005−489 is a nearby, $z = 0.07$, high-frequency peaked BL Lac object (HBL). A strong X-ray outburst was observed in November, 1998 (Remillard, 1998; Perlman et al., 1999). This source has also been detected at γ-ray energies by EGRET (Thompson et al., 1995). PKS 2005−489 exhibited a very flat radio spectrum throughout the ATCA monitoring program, showing no evidence for opacity changes in variable components. This is consistent with the finding of Aller (1999), that BL Lac objects from the UMRAO monitoring program tend to show little change in spectral index during

activity, indicating a transparent emission region, while quasars commonly show effects of self-absorption. The original Parkes catalog flux densities for PKS 2005−489 (Wall et al., 1975) are 1.1 Jy at 2.7 GHz, and 1.2 Jy at 5 GHz, showing that a flat radio spectrum is a long-term property of this source. The fluctuations observed in both the total and polarized flux density of PKS 2005−489 during the ATCA monitoring program are somewhat undersampled.

PKS 2149−306

Peterson & Bolton (1973) identified PKS 2149−306 with a 17th magnitude quasar. The Parkes catalog flux densities are 1.3 Jy at 2.7 GHz, and 1.2 Jy at 5 GHz (Shimmins & Bolton, 1974). This source was one of the least variable of those monitored in the ATCA program, showing only a few percent modulation during the three years. At $z = 2.345$ (Wilkes et al., 1983), it is also the highest redshift source observed in the present program. Not detected by EGRET.

PKS 2155−304

The original Parkes catalog flux densities for PKS 2155−304 are 0.34 Jy at 2.7 GHz, and 0.31 Jy at 5 GHz. This source is an HBL and a strong X-ray source, which was subject to an intensive multiwavelength campaign in 1994 (Pesce et al., 1997). It is also an EGRET blazar and a candidate for detection of TeV γ-rays. During the 1994 multiwavelength campaign, no correlation was observed between the radio variability and the higher energy variability (Pesce et al., 1997). PKS 2155−304 showed marginal IDV in the ATCA IDV Survey of Kedziora-Chudczer et al. (2001b), therefore scintillation may be important for this source. During the ATCA monitoring program, the flux density varied between 0.3 and 0.5 Jy.

3C 446 (B2223−052)

3C 466 is a highly polarized quasar (Moore & Stockman, 1981) and has been well-studied from X-ray to radio wavelengths. This source showed no significant variability at 1.4 GHz during the ATCA monitoring, however the light curves show the beginning of an outburst at the higher frequencies. 3C 466 is not an EGRET source.

CTA 102 (B2230+114)

CTA 102 is a rather "famous" quasar which has been well-studied at radio wavelengths for many years (e.g. Kellermann & Pauliny-Toth, 1968). It showed little variability at 1.4 GHz during the ATCA monitoring program, and observations over many years are clearly required to probe time-scales of radio variability in this source. CTA 102 has been observed in the UMRAO monitoring program (e.g. Aller et al., 1985). It is also an EGRET blazar.

PKS 2243−123

The Parkes catalog flux densities for PKS 2243−123 are 2.7 Jy at 2.7 GHz, and 2.4 Jy at 5 GHz (Bolton et al., 1975). A quasar at $z = 0.63$ (Browne et al., 1975), this source is also an optical variable with $> 3\%$ optical polarization (Impey & Tapia, 1988). PKS 2243−123 was quite variable during the ATCA monitoring program, changing by 1 Jy in 1.4 years at 8.6 GHz. The polarized flux density is also quite variable at the higher frequencies. Optical depth effects are evident in the observed variations at different frequencies. Not an EGRET detection.

3C 454.3 (B2251+158)

Another EGRET-detected blazar (Thompson et al., 1995), 3C 454.3 is a well-studied, high-optically polarized quasar. It has shown optical variability on a time scale of hours (e.g. Angione, 1971), but shows no evidence for radio IDV. 3C 454.3 is a very strong radio source which showed a slightly optically thin spectrum for most of the ATCA monitoring program.

4.4 Discussion

Radio monitoring of blazar variability has already yielded a great deal of information on jets in radio-loud AGN (e.g. Aller et al., 1996; Valtaoja, 1996, and references therein). Connecting variability in different bands across the electromagnetic spectrum would test a number of models, as discussed in Section 1.2.1, hence the recent emphasis on ground-based monitoring in conjunction with satellite experiments to observe high-energy X- and γ-ray emission.

Some new radio results have been presented in this chapter; variability in many of the southern sources has not previously been studied in detail. The ATCA allows accurate and efficient measurements of both total and polarized flux density, with broad-band, instantaneous frequency coverage. The best instruments for studies of long-term variability in strong radio blazars, however, have proved to be dedicated telescopes, such as the University of Michigan 26 m antenna (e.g. Aller et al., 1985). In the radio band, many sources show outbursts on time-scales of years, and hence monitoring over many years is necessary to properly analyse the radio variability.

Much of the observed long term variability has been found to be consistent with models of shocks propagating in relativistic jets (e.g. Hughes et al., 1989; Marscher, 1996). For many of the sources observed here, opacity effects are evident in the light curves: outbursts peak at later times, and with lower amplitude, towards longer wavelengths. This is generally explainable as being due to shocks which originate in the compact inner jet which is opaque to radio emission, and propagate along the jet. The cm wavelength variability is then just the tail-end of the huge releases of energy observed in many blazars at higher frequencies. Some sources show simultaneous variability across the observed frequency range, perhaps indicating that in some sources, shocks form in parts of the jet which are optically thin (see, e.g. Aller, 1999).

The Galactic interstellar medium (ISM) also plays an important role in cm wavelength variability. Extreme scattering events (ESEs; Fiedler et al. 1987; see Section 1.3.6), although rare, have been observed in some of these sources in other monitoring programs. A much more common phenomenon is interstellar scintillation (ISS). Refractive and weak scintillations are important for very compact sources across the whole range of frequencies observed here, 1.4–8.6 GHz.

For studies of radio intraday variability, it is the bigger telescopes which are better. Detailed IDV studies are very difficult, if not impossible, using a small antenna. The 100 m telescope of the MPIfR in Bonn, Germany, has been used to study IDV sources for almost two decades (e.g Heeschen et al., 1987; Quirrenbach et al., 1992), and more recently, interferometers such as the ATCA, the VLA, and the Westerbork Synthesis Radio Telescope (WSRT) have been used for IDV studies (e.g. Kedziora-Chudczer et al., 2001b; Quirrenbach et al., 2000; Dennett-Thorpe & de Bruyn, 2000). Recently, the weight of evidence has swung heavily in favour of interstellar scintillation as the principal cause of cm wavelength IDV. The next two chapters present detailed investigations of IDV sources using the ATCA.